Event-Based Non-Intrusive Home Current Measurement Using Sensor Array

Juncheng Wang, *Student Member, IEEE*, Guangchao Geng, *Member, IEEE*, Kun-Long Chen, *Member, IEEE*, Hao Liang, *Member, IEEE*, and Wilsun Xu, *Fellow, IEEE*

***Abstract*—This paper presents a novel method for non-intrusive home current measurement using an array of magnetic field sensors. It is specifically designed for measuring the real-time currents on three wires, including two hot wires and one neutral wire, enclosed in the electric conduits of North American homes. The key idea is to extract information from appliance state changing events captured by sensor measurement changes. Since each detected event only corresponds to two wires between which the state-changing appliance is connected, the events can be clustered according to the wire connections. Wire position identification is formulated as a nonlinear least square problem and is efficiently solved. Then, real-time current measurement is achieved by using the trans-impedance matrix built based on the solved wire positions and the sensor parameters obtained from the manufacturing process. The proposed method is evaluated by extensive laboratory and field tests.**

***Index Terms*—Event detection and clustering, magnetic field sensor, non-intrusive current measurement, nonlinear least square, sensor array.**

NOMENCLATURE

Set and Dimension

$\mathbb{S}_S, n_s$	Magnetic sensors.
$\mathbb{S}_C, n_c$	Wires.
$\mathbb{S}_E, n_e$	Detected events.
$\mathbb{S}_{E_k}, n_{e_k}$	Events clustered as type k.
$\mathbb{S}_T, n_t$	Types of events.
$\mathbb{S}_U, n_u$	Events used to solve the NLLS problem.

Parameters

x_s, y_s	Calibrated sensor coordinates.
g_s	Calibrated amplification factor.
θ_s	Calibrated sensing direction.
V_s	Sensor measurement.
r_c	Electric conduit inner radius.

Variables

x_c, y_c	Wire coordinates.
I_c	Wire current.
$g_k^{e_k}$	Current unbalance ratio for type k event.

Manuscript received December 21, 2016; revised March 17, 2017; accepted April 20, 2017. Date of publication April 25, 2017; date of current version October 19, 2018. Paper no. TSG-01787-2016. *(Corresponding author: Juncheng Wang.)*

J. Wang, K.-L. Chen, H. Liang, and W. Xu are with the Department of Electrical and Computer Engineering, University of Alberta, Edmonton, AB T6G 1H9, Canada (e-mail: ju4@ualberta.ca; poplone0602@gmail.com; hao2@ualberta.ca; wxu@ualberta.ca).

G. Geng is with the College of Control Science and Engineering, Zhejiang University, Hangzhou 310027, China (e-mail: ggc@zju.edu.cn).

Color versions of one or more of the figures in this paper are available online at http://ieeexplore.ieee.org.

Digital Object Identifier 10.1109/TSG.2017.2698035

I. INTRODUCTION

HOME current measurement provides basic but vital information for advanced home energy monitoring and management, which is a critical enabling technology for smart homes [1]. Accurate and easy-to-implement home current measurement can enable various smart home applications such as non-intrusive load monitoring (NILM) [2], home energy management [3] and demand response management [4]. Since it is not safe to install current measurement devices inside a home service panel, existing approaches rely on the measurements on incoming wires which are commonly above the service panel and enclosed in a plastic electric conduit. Therefore, the major technical challenge of home current measurement has been identified as the inaccessibility of individual wires with unknown positions in the electric conduit [5].

Current sensing technologies featured by low-cost wide-range current sensors are applied to various industrial applications [6]. Magnetic field sensors, like coil sensors [7] and Hall effect sensors [8], can be deployed around a single wire to detect the magnetic fields and measure the current inside. However, it is more complicated to measure the currents of multi-wires since the sensed magnetic fields are cross-coupled. Reference [9] provides an approach to decouple the cross-coupled magnetic fields by building the relationship between sensor measurements and wire currents with known geometries of wires and locations of detectors. An apparatus is designed in [10] to measure two-wire currents with known wire positions. However, such measurements are not accurate enough to measure enclosed wires with unknown geometric information. An optimization problem with redundant sensors is formulated in [11] to achieve non-contact measurements. Evolutionary algorithm is used in [12] to measure three phase currents with ten sensors. A non-intrusive home current measurement problem is investigated in [13]. The proposed approach uses a dedicated on-site calibrator to assist the identification of wire positions. Yet, how to eliminate the use of on-site calibrator and how to reduce the number of sensors for current measurement are still open issues which require extensive research.

Distinguished from the existing approaches, this work is particularly based on a unique observation of the service panels of North American homes, that is, among the three wires (i.e., two hot wires with $\pm 120V$ and the neutral wire), significant current changes caused by the state changes (i.e., turning on/off or varying operation modes) of individual appliances only occur on two out of the three wires. This property enables us to extract the sensor measurements associated with each pair of two wires rather than all three wires, which greatly simplifies the non-intrusive home current measurement problem. Since the unbalanced load current returns to the service transformer through both neutral and ground wires via the neutral-ground bond at the service panel, the current unbalance ratio derived from the current return ratio concept in [14] is used to model the unequal current changes in two wires, when an appliance state changing event happens. Based on this model, we can detect the appliance state changing events through sensor measurement changes, and subsequently, cluster the events according to their wire connections by using cosine similarity as a distance index. Then, the positions of the three wires can be identified by formulating a nonlinear least square (NLLS) problem, which is efficiently solved by the state-of-the-art nonlinear programming (NLP) algorithm. For real-time measurement, the currents on the wires are calculated using the transimpedance matrix established based on the wire position information and sensor parameters. Extensive mathematical analysis and experimental results indicate that, six sensors are sufficient for the proposed event-based non-intrusive home current measurement method, without the requirement of a dedicated on-site calibrator. The main contributions of this paper are fourfold:

1) An analytical model is developed to simplify the home current measurement problem based on the definition of appliance state changing events and current unbalance ratio, such that the number of magnetic field sensors can be significantly reduced;
2) An event detection method is developed based on sensor measurements, and the detected events are clustered into types with different wire connections by using cosine similarity as a distance index;
3) An NLLS problem is formulated for wire position identification and is efficiently solved based on the state-of-the-art NLP algorithm;
4) The proposed method is validated through extensive laboratory and field tests. Experimental results indicate that the current measurement errors of the two hot wires are below 5%, which is sufficiently accurate for most of the aforementioned smart home applications.

The remainder of this paper is organized as follows. Section II provides an overview of the non-intrusive home current measurement technique. Section III describes the proposed event-based non-intrusive home current measurement method. The experimental results are presented Section IV, followed by the concluding remarks in Section V.

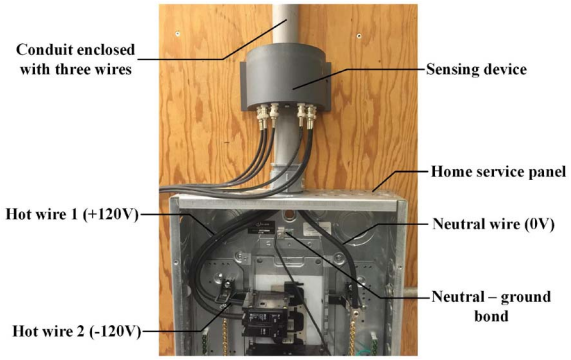

Fig. 1. The sensing device deployed at home service panel.

II. Non-Intrusive Home Current Measurement

In this section, we present an overview of the non-intrusive home current measurement technique. A typical North American home service panel is shown in Fig. 1, which leads $120V$ and $240V$ power from service transformer to home appliances. Three wires are enclosed in the incoming conduit (commonly used nonmetallic polyvinyl chloride (PVC) material) including two hot wires and one neutral wire carrying $+120V$, $-120V$ and $0V$ voltages, respectively. The neutral wire is grounded through neutral-ground bond at the service panel for ground fault protection. In this paper, the two hot wires and one neutral wire are named as A, B and N, respectively, for convenience.

A. Home Appliance Wire Connection

Most of the home appliances like microwave oven, induction cooker, fan, electric kettle and so on are connected through electric sockets to $120V$ voltage source. Some high-power appliances like kitchen stove, air conditioner, refrigerator and so on need $240V$ voltage to operate. An $120V$ voltage powered appliance is connected between either $A-N$ or $B-N$, while a $240V$ powered appliance is connected between $A-B$. Due to the neutral-ground bond at the service panel, the unbalanced load current I_u returns to the service transformer through either the neutral wire (with current I_n) or the grounding branch (with current I_g). A current return ratio $K = \Delta I_n / \Delta I_u$ is defined in [14] and can be used to characterize the difference between neutral and load currents. Since K is a function of the network impedance parameters and could vary if the impedance parameters change, a general variable called current unbalance ratio $g_k^{e_k}$ $(k \in \mathbb{S}_T, e_k \in \mathbb{S}_{E_k})$ is used in this paper to represent the inequality of the changed two wire currents when an appliance state change happens, to be introduced in Section III-A.

If the operating state of an appliance changes while the states of other appliances stay unchanged, only the currents of the two wires between which the appliance is connected can change, while the current of the remaining wire keeps constant. For example, as shown in Fig. 2, if the electric kettle connected between $A-N$ is turned on, I_a and I_n change by ΔI_{an} and $-\Delta I_{an} + \Delta I_g$, respectively, while I_b stays unchanged. On the

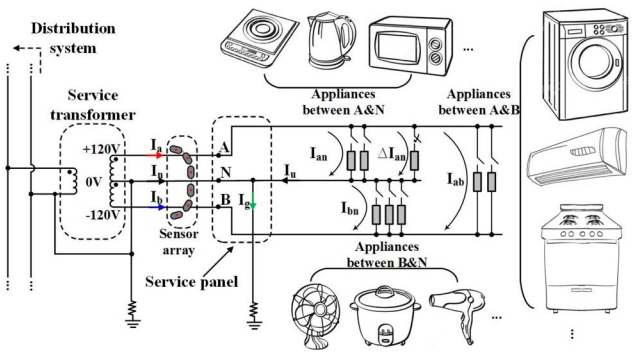

Fig. 2. Home appliance wire connections and state changing.

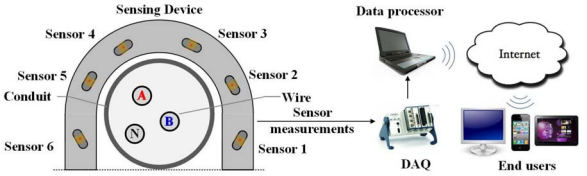

Fig. 3. The sensing device layout.

other hand, for the state change of an appliance connected between $A-B$, the changed currents are equal in magnitudes ($\Delta I_a = -\Delta I_b = \Delta I_{ab}$). This feature is later used to simplify the non-intrusive home current measurement problem.

B. Sensing Device

The sensing device is designed with a U shape shell that could be easily clamped on the conduit. The magnetic field sensors measuring the magnetic flux densities surrounding the conduit are shown in Fig. 3. Six coil sensors are placed with approximately equal intervals in the device to fully utilize the spatial diversity. The sensing device is connected to a data acquisition (DAQ) system and a PC for data processing. The current measurement results can be further uploaded and displayed on an Internet website for end users to access through electronic devices [13]. The estimated hardware cost of the sensing device is about $40 U.S.

C. Model of Sensed Magnetic Field

An *AC* current in a long straight wire generates a magnetic field around it according to the Biot-Savart law. The resultant magnetic field at the sensing position is proportional to the current magnitude and inversely proportional to the distance between the sensing point and wire position, on condition that the distance is much smaller than the wire length. The mixed magnetic field at a sensing point generated by multiple wires follows the superposition theory. The sensor parameters in terms of physical sensing position (x_{si}, y_{si}), measurement direction θ_{si} and circuit amplification factor g_{si} of the i-th sensor can be obtained from the manufacturing process and are known parameters in this paper.

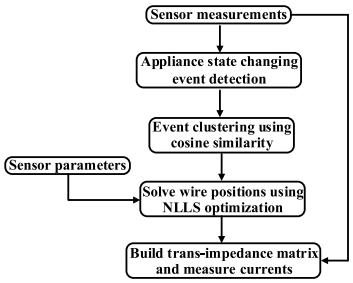

Fig. 4. Flow chart of the proposed event-based non-intrusive home current measurement method.

The number of sensors is denoted as n_s and the definitions of the parameters used in this paper are shown in the Nomenclature. The relationship between sensor measurements V_{si} $(i \in \mathbb{S}_s)$ and wire currents I_{cj} $(j \in \mathbb{S}_c)$ can be expressed in a matrix form as follows [15]:

$$\left[V_{si}\right]_{n_s\times 1} = \left[Z_{ij}\right]_{n_s\times 3} \times \left[I_{cj}\right]_{3\times 1}. \tag{1}$$

In (1), the trans-impedance matrix $\left[Z_{ij}\right]_{n_s\times 3}$ is the key of current measurement, where the element Z_{ij} for the i-th sensor and j-th wire can be obtained based on sensor and wire geometrical parameters as shown in (2) at the bottom of this page. Then, the i-th sensor measurement V_{si} is given by

$$V_{si} = \sum_{j\in\mathbb{S}_c} Z_{ij} I_{cj}, \quad \forall i \in \mathbb{S}_s. \tag{3}$$

III. Event-Based Current Measurement Method

The flow chart of the proposed event-based non-intrusive home current measurement method is shown in Fig. 4. Appliance state changing events are detected to extract sensor measurements generated by the changed currents. The extracted events are further clustered using cosine similarity as difference index according to the different vector patterns of extracted sensor measurements, which correspond to different wire connections of the state changing appliances. In particular, a total of three types of events (E_{an}, E_{bn}, E_{ab}) can be clustered because appliances are connected between either $A-N$, $B-N$ or $A-B$. Unknown wire positions are solved based on NLLS optimization. After building trans-impedance matrix using the solved wire positions and calibrated sensor information to build the relationship between sensor measurements and wire currents, real-time current measurement is achieved by simple matrix computation.

$$Z_{ij} = g_{si}\frac{\mu_0}{2\pi}\frac{(x_{si}\cos\theta_{si} - y_{si}\sin\theta_{si})(x_{si}-x_{cj}) + (y_{si}\cos\theta_{si} + x_{si}\sin\theta_{si})(y_{si}-y_{cj})}{\sqrt{x_{si}^2+y_{si}^2}\left[(x_{si}-x_{cj})^2 + (y_{si}-y_{cj})^2\right]} \quad \forall i \in \mathbb{S}_s, \ \forall j \in \mathbb{S}_c \tag{2}$$

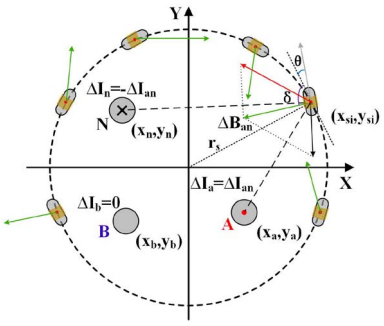

Fig. 5. Magnetic fields generated by the two wires of an event.

A. Event-Based Problem Simplification

According to (1), a total of nine unknown variables including wire positions (x_a, y_a), (x_b, y_b), (x_n, y_n) and wire currents I_a, I_b, I_n need to be solved using sensor measurements V_{si} $(i \in \mathbb{S}_s)$. Thus, in the existing approach, at least nine sensors should be used to solve the nonlinear equation system [12]. However, by detecting the appliance state changing events and subtracting the sensor measurements at the pre-event point V_{si}^{pre} $(i \in \mathbb{S}_s)$ and post-event point V_{si}^{post} $(i \in \mathbb{S}_s)$ as (4), the changed sensor measurements ΔV_{si} $(i \in \mathbb{S}_s)$ generated only by the changed appliance currents flowing through two of the three wires can be extracted as (5).

$$\left[\Delta V_{si}\right]_{n_s\times 1} = \left[V_{si}^{post}\right]_{n_s\times 1} - \left[V_{si}^{pre}\right]_{n_s\times 1} \tag{4}$$

$$= \left[Z_{ij}\right]_{n_s\times 3} \times \left(\left[I_{cj}^{post}\right]_{3\times 1} - \left[I_{cj}^{pre}\right]_{3\times 1}\right). \tag{5}$$

Take a state changing appliance connected between $A-N$ as an example (e.g., the turn-on event of an electric kettle as described in Section II-A). As shown in Fig. 5, phase B current I_b has no impact on the extracted sensor measurements since $\Delta I_b = 0$. Mathematically, for the state changing event of an appliance connected between $A-N$ (denoted by e_{an}), we have

$$\left[\Delta V_{si}^{e_{an}}\right]_{n_s\times 1} = \left[Z_{ij}\right]_{n_s\times 3} \times \begin{bmatrix} \Delta I_{an}^{e_{an}} \\ 0 \\ -\Delta I_{an}^{e_{an}} + \Delta I_g^{e_{an}} \end{bmatrix}$$

$$= \left[Z_{ij}\right]_{n_s\times 3} \times \begin{bmatrix} \Delta I_{an}^{e_{an}} \\ 0 \\ -g_{an}^{e_{an}} \times \Delta I_{an}^{e_{an}} \end{bmatrix}. \tag{6}$$

Since each appliance can be connected between either $A-N$, $B-N$, or $A-B$, a total of three types of events can be extracted. Note that the event clustering process proposed in this paper does not assume the wires to which the appliances are connected, since such information is unknown for the non-intrusive home current measurement. Besides, the current return ratio (K) [14] may vary slightly when the network impedance parameters change. Therefore, we define a general variable called the current unbalance ratio $g_k^{e_k}$ $(k \in \mathbb{S}_T, e_k \in \mathbb{S}_{E_k})$ in this paper, to characterize the inequality between neutral and load current changes. The ratio is an unknown variable for each event and needs to be determined. In general, we have $g_{an}^{e_{an}} \approx g_{bn}^{e_{bn}} \neq 1$ and $g_{ab}^{e_{ab}} \approx 1$ if the changes of network impedance parameters are not significant. The corresponding sensor measurement changes for the three types of events are given by

$$\left[\Delta V_{si}^{e_{an}}\right]_{n_s\times 1} = \left[Z_{ia}, -Z_{in}\right]_{n_s\times 2} \times \begin{bmatrix} \Delta I_{an}^{e_{an}} \\ g_{an}^{e_{an}} \times \Delta I_{an}^{e_{an}} \end{bmatrix} \tag{7}$$

$$\left[\Delta V_{si}^{e_{bn}}\right]_{n_s\times 1} = \left[Z_{ib}, -Z_{in}\right]_{n_s\times 2} \times \begin{bmatrix} \Delta I_{bn}^{e_{bn}} \\ g_{bn}^{e_{bn}} \times \Delta I_{bn}^{e_{bn}} \end{bmatrix} \tag{8}$$

$$\left[\Delta V_{si}^{e_{ab}}\right]_{n_s\times 1} = \left[Z_{ia}, -Z_{ib}\right]_{n_s\times 2} \times \begin{bmatrix} \Delta I_{ab}^{e_{ab}} \\ g_{ab}^{e_{ab}} \times \Delta I_{ab}^{e_{ab}} \end{bmatrix} \tag{9}$$

where $e_{an} \in \mathbb{S}_{E_{an}}$, $e_{bn} \in \mathbb{S}_{E_{bn}}$ and $e_{ab} \in \mathbb{S}_{E_{ab}}$.

As we can see, by extracting appliance state changing events, the equations are greatly simplified and only consist of six unknown variables each. For example, the equation of an event happening between $A-N$ (corresponding to (7)) consists of six unknown variables: x_{ca}, y_{ca}, x_{cn}, y_{cn}, $\Delta I_{an}^{e_{an}}$ and $g_{an}^{e_{an}}$. Also, according to (6), the extracted sensor measurements of the same type of events are linearly dependent, since the current changes happen on the same set of two wires. For example, denoting the two events happening between $A-N$ as e_{an} and e'_{an}, respectively, we have

$$\left[\Delta V_{si}^{e_{an}}\right]_{n_s\times 1} = \gamma\left[\Delta V_{si}^{e'_{an}}\right]_{n_s\times 1}, \ \forall e_{an}, e'_{an} \in \mathbb{S}_{E_{an}} \tag{10}$$

where the coefficient γ is a (positive or negative) real number and is given by

$$\gamma = \Delta I_{an}^{e_{an}} / \Delta I_{an}^{e'_{an}}. \tag{11}$$

To establish the trans-impedance matrix $\left[Z_{ij}\right]_{n_s\times 3}$, at least two linearly independent events need to be detected to calculate the three wire physical positions. Any two of the three types of events are linearly independent as shown in (12).

$$\operatorname{rank}\begin{bmatrix} \Delta I_{an}^{e_{an}} & 0 & \Delta I_{ab}^{e_{ab}} \\ 0 & \Delta I_{bn}^{e_{bn}} & -g_{ab}^{e_{ab}} \times \Delta I_{ab}^{e_{ab}} \\ -g_{an}^{e_{an}} \times \Delta I_{an}^{e_{an}} & -g_{bn}^{e_{bn}} \times \Delta I_{bn}^{e_{bn}} & 0 \end{bmatrix} = 2. \tag{12}$$

A more effective way to obtain the wire positions is to solve a combined equation system which consists of different types of events. The number of effective observations provided by sensor measurements should be no less than the number of unknown variables based on the principle of least square [16]. Denote the number of linearly independent event types as n_d. In total, there are six unknown variables of wire positions (i.e., (x_a, y_a), (x_b, y_b) and (x_n, y_n)) need to be determined. Since each type of event adds two more unknown current variables (i.e., ΔI_k and g_k, respectively), we have

$$n_d \times n_s \geq 2 \times n_d + 6. \tag{13}$$

Dividing both sides of (13) by n_d, the minimum number of sensors needed to solve the problem is given by

$$n_s \geq 2 + \frac{6}{n_d} = 5, \ \text{if } n_d = 2. \tag{14}$$

Thus, if at least two types of events are extracted, five sensors are needed to solve the equation system. Considering the sensor measurement errors, one redundant sensor is added to achieve better measurement accuracy. Therefore, a total of six sensors are installed in the sensing device.

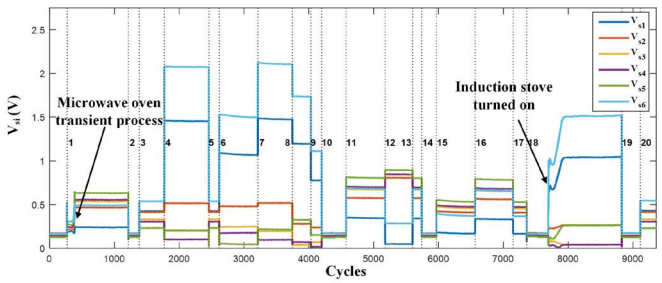

Fig. 6. An example of sensor measurement rms values.

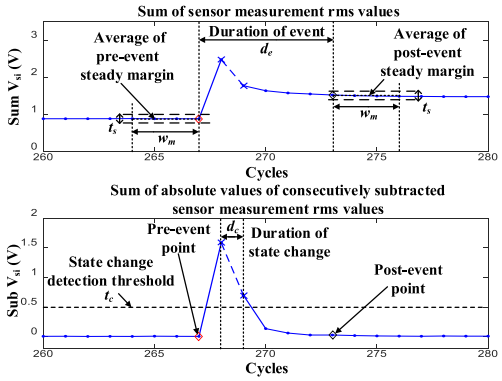

Fig. 7. An illustration of the event detection method.

B. Event Detection Using Sensor Measurements

Due to the linearity between sensor measurements and wire currents according to (6), appliance state changing events can be detected based on sensor measurements. An example of sensor measurements based on laboratory experiments is shown in Fig. 6. To extract the changed sensor measurements, only the appliance state changing events and the starting and ending points of them need to be detected.

An illustration of the event detection method is shown in Fig. 7. The sum of absolute values of consecutively subtracted sensor measurement rms values are used to detect appliance state changing duration, and the sum of sensor measurement rms values are used to confirm whether an event happens and determine the event duration. With the determined event duration, the changed sensor measurements generated only by the state changing appliance are extracted by subtracting the sensor measurements at pre-event and post-event points. Specifically, if the sum of absolute values of consecutively subtracted sensor measurement rms values is above the state change detection threshold t_c, it is considered as a potential event and the duration of state change d_c is determined. The pre-event and post-event steady margins with w_m cycles width are determined if all the sensor measurement rms values among the margins are within t_s limit of their average value. The pre-event and post-event points are the last and first data points of determined margins, respectively. To confirm if an event occurred, the sum of subtracted sensor measurement rms values between pre-event and post-event data points are calculated. The event is recorded if the difference is greater than a pre-specified threshold t_d considering the impact of

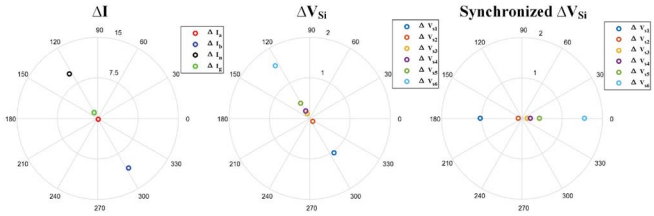

Fig. 8. Changed currents and extracted sensor measurements (event 5).

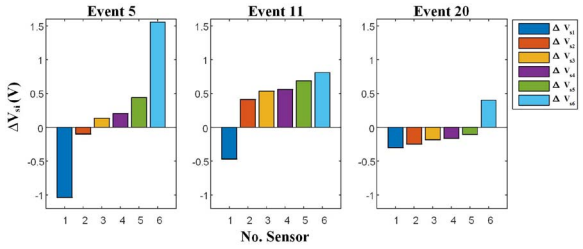

Fig. 9. Extracted sensor measurement patterns of different events.

sensor measurement noise and appliance current fluctuations. The length of event duration is limited within d_e cycles.

Using the above event detection method, the unstable, small or long-lasting appliance state changing events will not be extracted. An example of the event detection results is shown in Fig. 6. As we can see, a total of 20 events are extracted in around nine thousand cycles. Here, the transient process of microwave oven and the turn-on event of induction stove are not extracted due to their unstable and long-lasting state changes, respectively. All other events are extracted, with their IDs given in Fig. 6.

C. Event Clustering Using Cosine Similarity

The appliance state changing events are extracted by subtracting the data measured at pre-event and post-event points. Based on our analysis in (10) and (11), the extracted sensor measurements ΔV_{si} ($i \in \mathbb{S}_s$) of the same type of events should be linearly dependent and share the same or opposite phase directions. In particular, if two events are of the same type, the coefficient γ in (11) is a positive or negative real number. However, since the sensor amplifier circuits may not be exactly the same, it is necessary to synchronize ΔV_{si} ($i \in \mathbb{S}_s$). Specifically, the sensor measurement of an event with largest magnitude is selected to be the reference vector and is assigned with 0° or 180° phase angle depending on whether the pre-synchronized phase angle is less than 180° or not. The remaining sensor measurements are synchronized to the reference vector with the same or opposite phase angle and unchanged magnitudes. An example is shown in Fig. 8 for event 5 of Fig. 6.

For different types of events, the patterns of extracted sensor measurements ΔV_{si} are different. The extracted sensor measurements of three representative events are shown in Fig. 9, which happen between $B-N$, $A-N$, and $A-B$, respectively, with the changed currents shown in Fig. 10.

Therefore, the extracted sensor measurements generated by appliances connected between the same two wires should be

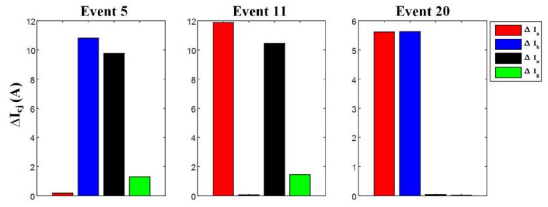

Fig. 10. Changed currents of different events.

clustered as one type of events. Cosine similarity measures the similarity between two vectors according to the angle between them. It is well suited for the event clustering task in this paper if we take the extracted sensor measurements as vectors. Consider two arbitrary events e and e', the cosine similarity between them is given by

$$D_{e,e'} = \left| \frac{\sum_{i\in\mathbb{S}_s} \Delta V_{si}^{e} \Delta V_{si}^{e'}}{\sqrt{\sum_{i\in\mathbb{S}_s} (\Delta V_{si}^{e})^2} \sqrt{\sum_{i\in\mathbb{S}_s} (\Delta V_{si}^{e'})^2}} \right|, \quad \forall e, e' \in \mathbb{S}_E. \tag{15}$$

where $\mathbb{S}_E = \mathbb{S}_{E_{an}} \cup \mathbb{S}_{E_{bn}} \cup \mathbb{S}_{E_{ab}}$ is the set of all events. For two events with the same type, the cosine similarity between them should be close to 1. Take two events happening between $A-N$ (e_{an} and e'_{an}) as an example. By substituting (10) and (11) into (15), we have

$$D_{e_{an},e'_{an}} = \left| \gamma / \sqrt{\gamma^2} \right| = 1, \ \ e_{an}, e'_{an} \in \mathbb{S}_{E_{an}}. \tag{16}$$

On the other hand, the cosine similarity between two events with different types are generally not close to 1. Therefore, a total of three groups of events can be clustered by using cosine similarity. An example is shown in Fig. 11 based on the sensor measurements in Fig. 6. The events of the same type are further sorted with a descending order of the sum of the absolute values of the extracted sensor measurements $\sum_{i\in\mathbb{S}_s} |\Delta V_{si}|$. The events with larger current changes will get higher priority for later wire position identification.

D. Wire Position Identification and Current Measurement

The trans-impedance matrix $\left[Z_{ij}\right]_{n_s\times 3}$ between sensor measurements and wire currents is critical for real-time current measurement. However, $\left[Z_{ij}\right]_{n_s\times 3}$ consists of unknown wire positions. After event detection and clustering, the combined

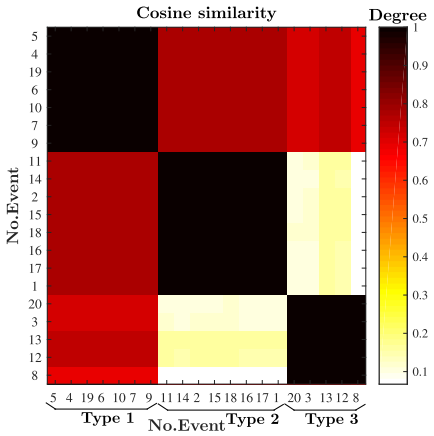

Fig. 11. Event clustering of extracted events.

equation system consisting of different types of events is built to solve the unknown wire positions. It is modelled as a NLLS optimization problem, which minimizes the difference between the summations of extracted sensor measurements $\Delta V_{si}^{e_k}$ ($i \in \mathbb{S}_s, k \in \mathbb{S}_T$) and calculated sensor measurements $\Delta V_{bi}^{e_k}$ ($i \in \mathbb{S}_s, k \in \mathbb{S}_T$) as shown in (17) at the bottom of this page, where $\mathbb{S}_T = \{E_{an}, E_{bn}, E_{ab}\}$ is the set of event types. The calculated sensor measurements for different types of events $\Delta V_{bi}^{e_k}$ ($i \in \mathbb{S}_s, k \in \mathbb{S}_T$) are obtained in (18)–(20), as shown at the bottom of this page, respectively. Several constraints are added for better identification performance. In particular, the wire coordinates are limited by the physical sizes of electric conduit (inner radius r_c) and wire (outer radius r_w) as shown in (21) at the bottom of this page. The distance between any two wires should be no less than the wire diameter d_c and smaller than the subtraction of wire diameter from electric conduit diameter ($2r_w$) as shown in (22) at the bottom of this page. The magnitudes of changed currents are limited by the maximum current of home appliances (ΔI_{max}) as shown in (23) at the bottom of this page, while the boundary of ΔV_{bi} is given by the voltage range of amplifier (V_{op}) as shown in (24) at the bottom of this page. The current unbalance ratio $g_k^{e_k}$ is a positive number with an upper bond g_{max} as shown in (25) at the bottom of this page.

By solving the NLLS problem, the trans-impedance matrix can be built based on the identified wire positions. According

$$\min \sum\nolimits_{i\in\mathbb{S}_S, k\in\mathbb{S}_T, e_k\in\mathbb{S}_{E_k}} \left(\Delta V_{si}^{e_k} - \Delta V_{bi}^{e_k}\right)^2 \tag{17}$$

$$\text{s.t.} \begin{cases} \forall i \in \mathbb{S}_s & \begin{cases} \forall e_{an} \in \mathbb{S}_{E_{an}}, \Delta V_{bi}^{e_{an}} = (Z_{ia} - g_{an}^{e_{an}} \times Z_{in}) \Delta I_{an}^{e_{an}} & (18) \\ \forall e_{bn} \in \mathbb{S}_{E_{bn}}, \Delta V_{bi}^{e_{bn}} = (Z_{ib} - g_{bn}^{e_{bn}} \times Z_{in}) \Delta I_{bn}^{e_{bn}} & (19) \\ \forall e_{ab} \in \mathbb{S}_{E_{ab}}, \Delta V_{bi}^{e_{ab}} = (Z_{ia} - g_{ab}^{e_{ab}} \times Z_{ib}) \Delta I_{ab}^{e_{ab}} & (20) \end{cases} \\ \forall j \in \mathbb{S}_c & \sqrt{(x_{cj})^2 + (y_{cj})^2} \le r_c - r_w & (21) \\ \forall j_1, j_2 \in \mathbb{S}_c, j_1 \ne j_2 & 2r_w \le \sqrt{(x_{cj_1} - x_{cj_2})^2 + (y_{cj_1} - y_{cj_2})^2} \le 2r_c - 2r_w & (22) \\ \forall k \in \mathbb{S}_T, \forall e_k \in \mathbb{S}_{E_k} & \begin{cases} \left|\Delta I_k^{e_k}\right| \le \Delta I_{max} & (23) \\ \forall i \in \mathbb{S}_s \ \ \left|\Delta V_{bi}^{e_k}\right| \le V_{op} & (24) \\ 0 < g_k^{e_k} < g_{max} \end{cases} \end{cases}$$

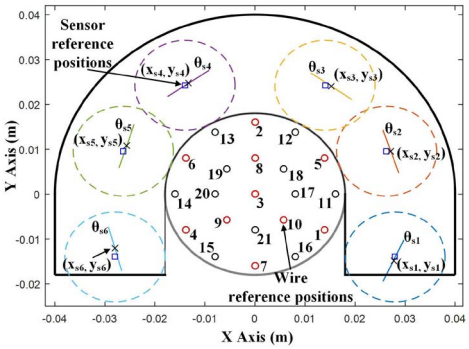

Fig. 12. Laboratory experiment layout.

TABLE I
SENSOR PARAMETERS

Sensors	$x_s(mm)$	$y_s(mm)$	g_s	$\theta_s(rad)$
1	27.69	−14.78	3.08	0.068
2	27.15	9.55	3.11	−0.020
3	15.24	24.07	3.17	−0.062
4	−13.16	24.71	3.03	0.121
5	−25.63	10.76	2.93	0.097
6	−27.97	−12.13	2.85	−0.144

TABLE II
EVENT DETECTION AND NLLS PARAMETERS

NLLS		Event Detection	
r_c	18 mm	t_d	0.5 V
r_w	1.8 or 3 mm	t_c	0.05 V
V_{op}	9 V	t_s	1 %
ΔI_{max}	20 A	w_m	3 $cycles$
g_{max}	5	d_e	8 $cycles$

to (1), real-time current measurement can be achieved as

$$\left[I_{cj}\right]_{3\times 1} = \left[Z_{ij}\right]^{-1}_{n_s\times 3} \times \left[V_{si}\right]_{n_s\times 1} \tag{26}$$

where $\left[Z_{ij}\right]^{-1}_{n_s\times 3}$ is the pseudo inverse of matrix $\left[Z_{ij}\right]_{n_s\times 3}$.

IV. EXPERIMENTAL RESULTS

The proposed event-based home current measurement method has been validated by extensive laboratory experiments and field tests. The laboratory experiments use three aluminum bars as wires inserted in a 3D printed wire holder with 21 reference positions as shown in Fig. 12. The sensor parameters x_s, y_s, θ_s, and g_s are shown in Table I, while the parameters used for event detection and solving NLLS are shown in Table II. The field tests are conducted at a residential house in Edmonton, AB, Canada.

A. Laboratory Experiments

The test bed is illustrated in Fig. 13. Two transformers are connected in series to generate $+120V$, $-120V$ and $0V$ voltages from two power sources. The maximum phase current is limited by the transformer capacity ($20A$). The currents I_a, I_b, I_n and I_g are measured using Fluke i1000s accurate current clamps as reference values. Common home appliances such as

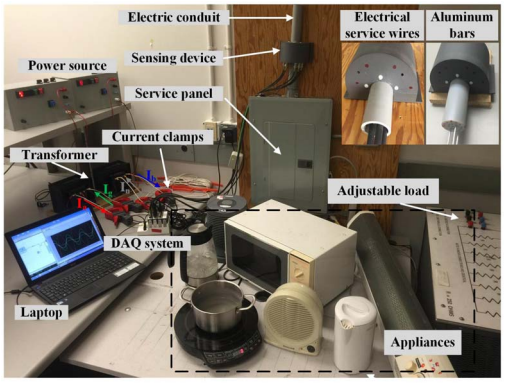

Fig. 13. Laboratory experiment test bed.

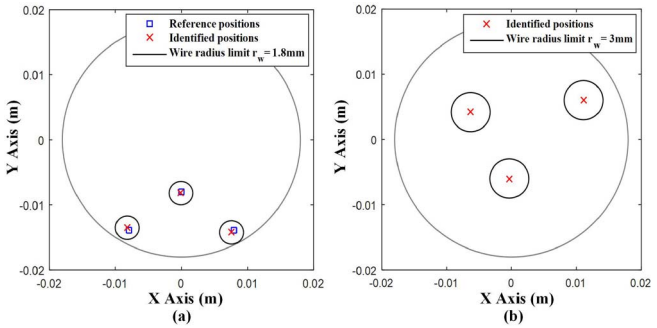

Fig. 14. Identified wire positions: (a) Laboratory test Case 7; (b) Field test.

microwave oven, induction stove, fan, electric kettle, and so on are connected to the $120V$ voltages and an adjustable resistive load is connected to the $240V$ voltage. Load changes are accomplished by turning on and off the appliances or varying the operation modes. The sensor measurements and reference currents are acquired by an NI-DAQ instrument and recorded by a laptop using LabVIEW data acquisition software.

The wire position solving task is modeled as an NLLS optimization problem formulated in AMPL and solved using KNITRO [17]. A PC configured with a 2.40-GHz Intel Core i7-4700MQ CPU and 8GB RAM is used for the wire position identification. A total of 15 cases with different wire positions and real appliances are used. The average currents of the 15 cases are $I_a \approx 9A$, $I_b \approx 7.5A$ and $I_n \approx 6A$, respectively. A total of 12 events, with 4 for each type, are used to solve NLLS optimization. On average, the wire positions are solved in 0.1750 second CPU time using the NLP algorithm.

An example of the wire positions solved in laboratory experiments are shown in Fig. 14 (a) and are compared with the reference positions. This case (i.e., case 7) corresponds to the worst case we found during our laboratory experiments (with the largest measurement errors). The three wires are gathered with positions A-21, B-15 and N-16 as defined in Fig. 12. We can see that, even for this worst case, the wire positions are solved with high accuracy. Based on the solved wire positions, real-time currents are obtained by matrix computation (26). The calculated currents are compared with the reference currents in Fig. 15. The absolute current measurement errors are shown in Fig. 16. As we can see, the absolute errors are below $1A$ for most of the cases.

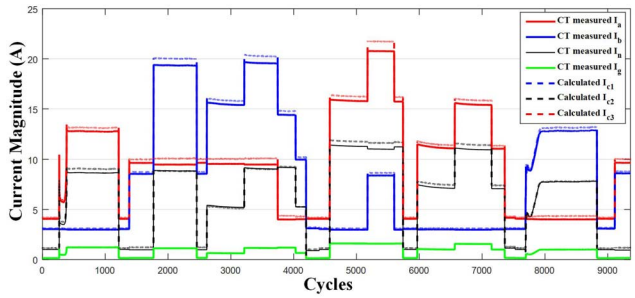

Fig. 15. Current measurement results of laboratory test Case 7.

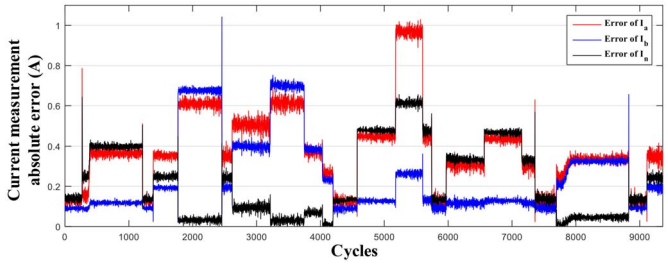

Fig. 16. Absolute errors of current measurements for laboratory test Case 7.

TABLE III
THE ACCURACY OF CURRENT MEASUREMENTS OF ALL CASES

Cases	Positions	Absolute Error (A)			Relative Error %		
		I_a	I_b	I_n	I_a	I_b	I_n
1	8, 9, 10	0.13	0.09	0.12	1.38	1.41	1.87
2	3, 7, 1	0.11	0.10	0.18	1.29	1.29	3.35
3	2, 6, 1	0.05	0.03	0.04	0.87	0.72	1.50
4	2, 3, 5	0.13	0.11	0.15	1.46	1.18	2.61
5	4, 2, 1	0.13	0.07	0.06	1.42	1.18	1.70
6	3, 15, 16	0.07	0.11	0.16	0.86	1.34	4.12
7	21, 15, 16	0.39	0.25	0.22	4.55	3.24	6.54
8	4, 9, 1	0.06	0.09	0.11	0.87	2.19	2.15
9	17, 15, 16	0.05	0.05	0.12	0.65	1.11	3.57
10	10, 20, 15	0.15	0.15	0.13	1.69	1.87	2.59
11	17, 21, 16	0.24	0.24	0.17	2.71	3.90	7.27
12	14, 19, 9	0.10	0.09	0.19	1.07	1.23	5.78
13	15, 19, 10	0.08	0.09	0.16	0.91	1.12	5.73
14	19, 2, 18	0.27	0.15	0.14	2.97	2.33	7.16
15	18, 9, 16	0.06	0.10	0.03	0.80	1.56	1.19

The accuracy of current measurements of all 15 cases in laboratory experiments is shown in Table III. The average absolute errors of measured currents are within 0.2*A* for most of the cases, and the average relative errors for I_a and I_b are within 4% in general. Due to smaller magnitude, I_n is measured with higher but less than 8% average relative error. All the laboratory experimental results indicate that accurate current measurements can be achieved by our proposed method for various combinations of wire positions.

B. Field Tests

The field tests are conducted at a residential house with the sensing device installed at the overhead service entrance point as shown in Fig. 17 (a). Nonmetallic PVC schedule 40 conduit with size 1-1/4 (35.052 mm inner diameter) is most commonly

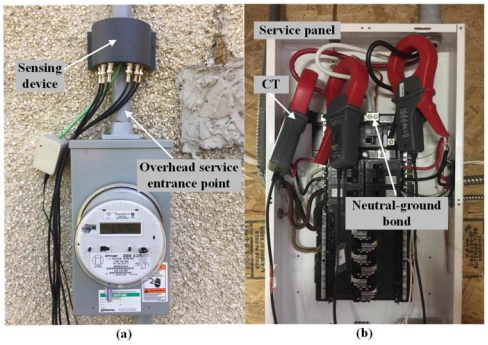

Fig. 17. Field test installation: (a) Sensing device at overhead service entrance point; (b) Reference currents measured by CTs at service panel.

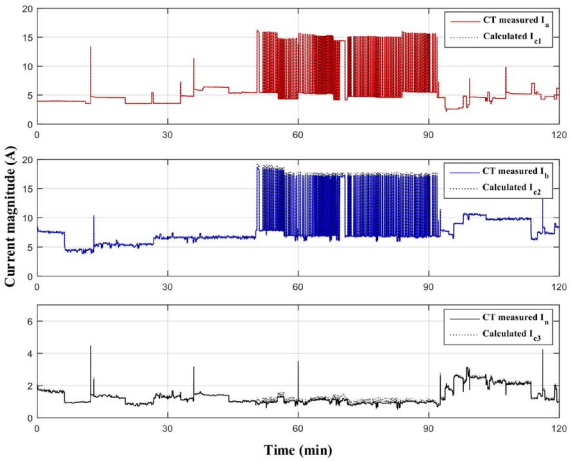

Fig. 18. Current measurement results of field test.

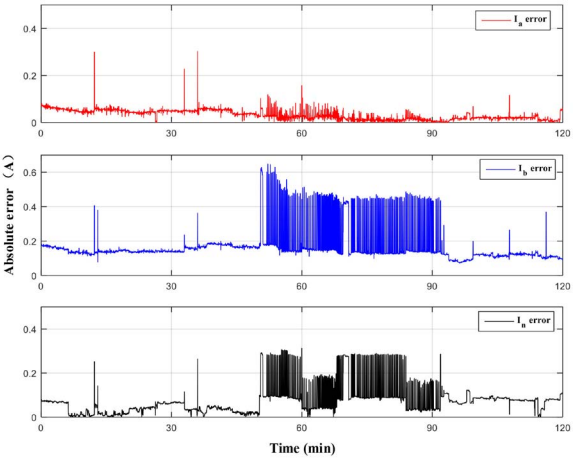

Fig. 19. Current measurement absolute errors of field test.

used in North American home service entrance. The conduit radius r_w of NLLS parameters can be changed accordingly if a conduit with other commonly used sizes (3/4 to 1-1/2) is tested. The reference values of currents are measured using three Fluke i1000s accurate current clamps in the main service panel as shown in Fig. 17 (b). A total of 18 events are extracted from a 10-min sensor measurement data and 12 of them (with 4 for each type of events) are used to solve the NLLS optimization problem. The NLLS parameters are same

as the ones used at laboratory experiments except that the wire radius limit r_w is set to 3 mm since most residential houses use service entrance wires with at least size 3 AWG (5.827 mm diameter). Based on the proposed method, the wire positions are solved with 2.141 seconds CPU time, and the results are shown in Fig. 14 (b). Then, the reference current and sensor measurement data are continuously recorded by two laptops from 6:00 p.m. to 8:00 p.m. In Fig. 18, the calculated wire currents are compared with the CT measured reference currents. The average relative errors are 0.68%, 2.14% and 6.35% for I_a, I_b and I_n, respectively. The current measurement absolute errors are shown in Fig. 19, with average values of $0.032A$, $0.169A$ and $0.073A$ for I_a, I_b and I_n, respectively. Based on the field test results, we can conclude that accurate home current measurements can be achieved based on our proposed method.

V. Conclusion

This paper has presented a novel, accurate and efficient method to achieve non-intrusive home current measurement. A low-cost sensing device with only six coil sensors has been designed to measure the currents of three wires, including two hot wires and one neutral wire, enclosed in the incoming conduit of home electric panel. The appliance state changing events are detected using sensor measurements and clustered. The wire position identification problem is formulated as an NLLS problem and efficiently solved using the state-of-the-art NLP algorithm. Extensive laboratory and field test results are presented to validated the proposed method. The applications of the sensing device to other types of conduits and cables will be investigated in our future work.

Acknowledgment

The authors would like to thank Pengfei Gao and Dr. Xiangguo Yang for helpful discussions.

References

[1] M. R. Alam, M. B. I. Reaz, and M. A. M. Ali, "A review of smart homes—Past, present, and future," *IEEE Trans. Syst., Man, Cybern. C, Appl. Rev.*, vol. 42, no. 6, pp. 1190–1203, Nov. 2012.

[2] Z. Wang and G. Zheng, "Residential appliances identification and monitoring by a nonintrusive method," *IEEE Trans. Smart Grid*, vol. 3, no. 1, pp. 80–92, Mar. 2012.

[3] M. Erol-Kantarci and H. T. Mouftah, "Wireless sensor networks for cost-efficient residential energy management in the smart grid," *IEEE Trans. Smart Grid*, vol. 2, no. 2, pp. 314–325, Jun. 2011.

[4] Z. Chen, L. Wu, and Y. Fu, "Real-time price-based demand response management for residential appliances via stochastic optimization and robust optimization," *IEEE Trans. Smart Grid*, vol. 3, no. 4, pp. 1822–1831, Dec. 2012.

[5] W. Xu, "Method and system for calibrating current sensors," U.S. Patent 8 718 964, May 2014.

[6] S. Ziegler, R. C. Woodward, H. H.-C. Iu, and L. J. Borle, "Current sensing techniques: A review," *IEEE Sensors J.*, vol. 9, no. 4, pp. 354–376, Apr. 2009.

[7] K. Draxler, R. Styblikova, J. Hlavacek, and R. Prochazka, "Calibration of Rogowski coils with an integrator at high currents," *IEEE Trans. Instrum. Meas.*, vol. 60, no. 7, pp. 2434–2438, Jul. 2011.

[8] K.-L. Chen and N. Chen, "A new method for power current measurement using a coreless Hall effect current transformer," *IEEE Trans. Instrum. Meas.*, vol. 60, no. 1, pp. 158–169, Jan. 2011.

[9] E. R. Olson and R. D. Lorenz, "Effective use of miniature multipoint field-based current sensors without magnetic cores," *IEEE Trans. Ind. Appl.*, vol. 46, no. 2, pp. 901–909, Mar./Apr. 2010.

[10] J. Zhang, Y. Wen, and P. Li, "Nonintrusive current sensor for the two-wire power cords," *IEEE Trans. Magn.*, vol. 51, no. 11, Nov. 2015, Art. no. 4005304.

[11] J. M. Libove and J. R. Singer, "Apparatus for measuring voltages and currents using non-contacting sensors," U.S. Patent 5 473 244, Dec. 1995.

[12] L. Meng, P. Gao, M. M. Haji, and W. Xu, "Magnetic sensor array-based AC current measurement for multiconductor cables using evolutionary computation method," *IEEE Trans. Instrum. Meas.*, vol. 64, no. 10, pp. 2747–2758, Oct. 2015.

[13] P. Gao, S. Lin, and W. Xu, "A novel current sensor for home energy use monitoring," *IEEE Trans. Smart Grid*, vol. 5, no. 4, pp. 2021–2028, Jul. 2014.

[14] W. Xu, J. R. Acharya, R. Torquato, and J. Yong, "A method to determine stray voltage sources—Part I: Concept and theory," *IEEE Trans. Power Del.*, vol. 30, no. 2, pp. 713–719, Apr. 2015.

[15] G. D'Antona, L. Di Rienzo, R. Ottoboni, and A. Manara, "Processing magnetic sensor array data for AC current measurement in multiconductor systems," *IEEE Trans. Instrum. Meas.*, vol. 50, no. 5, pp. 1289–1295, Oct. 2001.

[16] R. Fourer, D. M. Gay, and B. W. Kernighan, *AMPL: A Modeling Language for Mathematical Programming*. Cengage Learn., 2002. [Online]. Available: https://ampl.com/resources/the-ampl-book/

[17] R. H. Byrd, J. Nocedal, and R. A. Waltz, "KNITRO: An integrated package for nonlinear optimization," in *Large-Scale Nonlinear Optimization*, vol. 83. New York, NY, USA: Springer, 2006, pp. 35–59.

Juncheng Wang (S'15) received the B.S. degree in electrical engineering from Shanghai Jiao Tong University, Shanghai, China, in 2014. He is currently pursuing the master's degree with the Department of Electrical and Computer Engineering, University of Alberta, Edmonton, AB, Canada. His research interest includes smart grid, adaptive sensor array technique, and power system measurements.

Guangchao Geng (S'10–M'14) received the B.S. and Ph.D. degrees in electrical engineering from the College of Electrical Engineering, Zhejiang University, Hangzhou, China, in 2009 and 2014, respectively. He is currently a Post-Doctoral Fellow with the College of Control Science and Engineering, Zhejiang University, Hangzhou, China and the Department of Electrical and Computer Engineering, University of Alberta, Edmonton, AB, Canada. His research interest includes power system measurement, power system stability and control, and renewable energy integration.

Kun-Long Chen (S'11–M'15) received the B.S.E.E. degree from Feng-Chia University, Taichung, Taiwan, in 2004, and the M.S.E.E. and Ph.D. degrees from the National Taiwan University of Science and Technology, Taipei, Taiwan, in 2006 and 2011, respectively. Since 2015, he has been a Post-Doctoral Fellow with the University of Alberta, Edmonton, AB, Canada. His research interests include nonconventional voltage and current sensors, power metrology for smart grid, and nonintrusive load monitoring system.

Hao Liang (S'09–M'14) received the Ph.D. degree in electrical and computer engineering from the University of Waterloo, Waterloo, ON, Canada, in 2013. Since 2014, he has been an Assistant Professor with the University of Alberta. His research interests in the areas of smart grid, wireless communications, and wireless networking.

Wilsun Xu (M'90–SM'95–F'05) received the Ph.D. degree from the University of British Columbia, Vancouver, BC, Canada, in 1989. He is currently an NSERC/iCORE Industrial Research Chair Professor with the University of Alberta, Edmonton, AB, Canada. His research interests are power quality, power disturbance analytics, and power system measurements.